

## Bias correction of a novel European reanalysis data set for solar energy applications



Christopher W. Frank<sup>a,b,\*</sup>, Sabrina Wahl<sup>a,c</sup>, Jan D. Keller<sup>a,d</sup>, Bernhard Pospichal<sup>b</sup>, Andreas Hense<sup>c</sup>, Susanne Crewell<sup>b</sup>

<sup>a</sup> Hans-Ertel-Centre for Weather Research, Climate Monitoring and Diagnostics, Germany

<sup>b</sup> Institute of Geophysics and Meteorology, University of Cologne, Germany

<sup>c</sup> Meteorological Institute, University Bonn, Germany

<sup>d</sup> Deutscher Wetterdienst, Offenbach, Germany

### ARTICLE INFO

#### Keywords:

Global radiation  
Global horizontal irradiance  
Renewable energy  
Solar energy

### ABSTRACT

One of the major challenges during the transition phase of the energy system is to maintain the balance between energy supply and demand. Rising questions are often related to site mapping, variability, extremes and compensation effects for example. A fundamental source of information to answer these questions are high quality data sets of renewable energy related variables. As reanalyses provide all relevant data to assess wind and solar power generation over a long period of time (decades) in a gridded consistent way, they exhibit great potential in the field of renewable energy. A new regional reanalysis is COSMO-REA6, which covers the European domain over the years 1995–2014 with a horizontal resolution of about 6 km and a temporal resolution of 15 min. In this paper, we first assess the quality of the Global Horizontal Irradiance (GHI) provided by COSMO-REA6. High quality GHI measurements obtained through the Baseline Surface Radiation Network (BSRN) are used as reference and reveal systematic short comings in the reanalysis: (1) an underestimation of GHI in clear sky situations and (2) an overestimation of GHI in cloudy sky situations. In order to reduce these systematic regime dependent biases, a post-processing is developed. The applied post-processing method is a scaling based on orthogonal distance regressions for two different regimes, i.e., “clear sky” and “cloudy sky”. The two regimes are distinguished by the use of a transmissivity threshold. The post-processed GHI shows a significant reduction of the systematic biases and an improvement in representing the marginal distributions. A spatial cross-validation shows the applicability to the whole model domain of COSMO-REA6. Moreover, COSMO-REA6 as well as the post-processed GHI data reveal an added-value when compared to global reanalysis ERA-Interim and MERRA-2. The higher resolution reanalysis exhibits a significantly better performance of representing GHI variability, as well as biases, RMSE and other conventional scores. The post-processed GHI data are freely available for download.

### 1. Introduction

For a sustainable planning of the transition towards renewable energy production, the assessment of the solar energy potential and its variability has become more and more important (Kleissl, 2013). Due to the high spatial and temporal variability of solar radiation long-term data over large domains are necessary to identify potentials for the production of renewable energy and risks regarding the growing dependency on this form of power generation. In this respect also the co-variability of solar and wind energy becomes more important, as its anticorrelation is expected to balance the volatility of the individual sources to some extent (e.g. Bett and Thornton, 2016; Santos-Alamillos

et al., 2012; Grams et al., 2017). More extensive studies simulate the electricity network in order to study the electricity grid as a whole system. In this context, realistic meteorological data allow studying for example the future need of storage and/or back-up capacity (e.g. Heide et al., 2010; Mulder, 2014).

Traditionally, solar energy potential has been assessed from measured time series of solar irradiance at ground level. This is limited in its geographical distribution especially if high temporal resolution (< 1 h) and high quality measurements are concerned. Most frequently, the Global Horizontal Irradiance (GHI) also called Surface Solar Irradiance (SSI), is measured within the networks of meteorological services. A spatially extended view is provided by satellite estimates like the

\* Corresponding author at: Institute of Geophysics and Meteorology, University of Cologne, Germany.  
E-mail address: [cfrank@meteo.uni-koeln.de](mailto:cfrank@meteo.uni-koeln.de) (C.W. Frank).

HelioClim project by MINES ParisTech (Blanc et al., 2011) or the SARAH (Solar surfAce RADIation Heliosat) data set (Müller et al., 2015) produced by the Satellite Application Facility on Climate Monitoring (CM-SAF). They exploit geostationary satellite measurements to derive GHI for the full disk with up to hourly temporal and 0.05° spatial resolution. Atmospheric reanalyses compiled from observations and numerical weather prediction models provide not only GHI but rather the complete state of the atmosphere including the vertical profiles of wind, temperature, etc. in a physically consistent way. Therefore, these multi-year data sets which continually improve in resolution allow for a joint investigation of renewable energy resources (Bett and Thornton, 2016).

Global reanalyses that come at relatively coarse horizontal resolutions (40–100 km) are frequently used for investigating wind power generation (e.g. Staffell and Pfenninger, 2016; Ritter et al., 2015; Cannon et al., 2014; Kubik et al., 2013; Bett et al., 2013), but rarely for solar energy application (e.g. Boilley and Wald, 2015; Richardson and Andrews, 2014). One of the first applications by Lohmann et al. (2006) revealed large differences among two global reanalyses for monthly mean values at horizontal resolutions of about 200 km. When comparing two state-of-the-art reanalyses and satellite derived (Helio-Clim-1) daily solar irradiance with surface measurements across the globe Boilley and Wald (2015) find that a large part of the variability in surface radiation is not captured by the reanalyses. A reason for the deviation between reanalysis and measurements might arise from the difficulty to parameterize small scale processes related to clouds and aerosols including interaction with solar radiation.

The work of Richardson and Andrews (2014) indicated the potential of reanalyses in PV applications. For Ontario, Canada, Richardson and Andrews (2014) evaluated the use of NASA's global reanalyses MERRA (Rienecker et al., 2011) as input for PV modeling. They found that the modeled PV yields driven by MERRA results in just slightly higher errors than ground-measured driven results, despite relatively larger errors in the MERRA GHI data. Later, Pfenninger and Staffell (2016) showed a comparable performance of PV output simulations based on MERRA and MERRA-2 (Molod et al., 2015) compared to satellite estimates when aggregated to country-level.

One reason for the few studies using radiation from reanalyses for solar energy applications is the availability of the high quality satellite products. Many publications in the past are based on either solar or wind energy which caused the use of different data sources in the two fields. In the field of wind energy reanalyses products are frequently used (Rose and Apt, 2015) while for solar energy satellite products are found to be most accurate (Jia et al., 2013), at least compared to global reanalyses. To our best knowledge up to now high resolution regional reanalyses are not considered in the solar energy community. In recent times the question of co-variability and compensation effects of wind and solar energy become more and more important. Thus, the need of a common data source for both variables increased. Reanalyses provide wind and radiation in a physically consistent way in space and time. This is crucial for studying joint distributions, otherwise results and interpretation might be distorted due to physical inconsistencies. Using both variables from one source causes the question which reanalysis performs best in representing wind speed and radiation? This study addresses this question concerning the radiation part and takes regional reanalyses into account.

While global reanalyses mainly resolve clouds associated with synoptic disturbances, high resolution regional reanalyses have the potential to better describe smaller scale clouds associated with mesoscale processes like thunderstorms or orographic circulations and therefore are more suitable for solar energy applications. This paper investigates the quality of the novel European regional reanalysis COSMO-REA6 (Bollmeyer et al., 2015) available with a horizontal resolution of 6 km over a time period of 20 years and a temporal resolution of 15 min. Evaluation of COSMO-REA6 meteorological variables such as precipitation, temperature and wind speed (Wahl et al., 2017; Bollmeyer et al., 2015; Kaiser-Weiss et al., 2015; Borsche et al., 2016; Henckes

et al., 2018) has already shown a superior performance with respect to the European Centre for Medium-range Weather Forecasting (ECMWF) Re-Analysis Interim data set (ERA-Interim, Dee et al., 2011) but the representation of radiation has not been addressed so far.

An even higher resolution data set is available for Central Europe with a horizontal grid spacing of 2 km (COSMO-REA2, Wahl et al., 2017) albeit for a much shorter time period of seven years (2007–2013). However, due to its larger range of applicability, e.g., cross-country energy trading, we focus on the long-term European data set COSMO-REA6.

With this paper we focus on the following questions:

1. How accurate is COSMO-REA6 GHI compared to ground observations?
2. Does COSMO-REA6 GHI improve upon global reanalyses, i.e. ERA-Interim and MERRA-2, in bias and variability metrics?
3. Can the expected biases and deviations be corrected with a post-processing algorithm?

In order to address these questions the paper is structured as follows. Section 2 describes the reanalysis and observational data sets. A quality assessment of GHI from reanalyses is given in Section 3 which reveals some systematic deficits under clear and cloudy conditions. Therefore a post-processing procedure to correct these issues is developed in Section 4. An evaluation, including a cross-validation, of the post-processed radiation fields is presented in Section 5. Section 6 summarizes our findings followed by the conclusions in Section 7.

## 2. Data sets

### 2.1. COSMO-REA6

COSMO-REA6 has been developed and produced within the Climate Monitoring Branch of the Hans-Ertel-Centre for Weather Research<sup>1</sup> and is based on the Consortium for Small-Scale Modelling (COSMO) limited-area model (Schättler and Doms, 2011), which is part of the operational NWP model chain of the German Meteorological Service (DWD). It is a 20-year regional atmospheric reanalysis covering the European CORDEX EUR-11 domain with a horizontal resolution of 0.055° (approximately 6 km, see Fig. 1) and 40 vertical levels in terrain following coordinates. 3D model variables are archived every hour and 2D variables every 15 min. The most important variables, e.g. GHI, wind speed at the six lowest model level, can be downloaded via ftp (<http://reanalysis.meteo.uni-bonn.de>). In the reanalysis, a continuous nudging scheme is used to assimilate a wealth of observations into the model allowing for a detailed but temporally smooth representation of the prognostic variables (for further information the reader is referred to Bollmeyer et al., 2015).

The COSMO reanalyses uses the radiation scheme by Ritter and Geleyn (1992) based on the  $\delta$ -two-stream approximation. The scheme is called every 15 min and calculates how solar radiation is modified in the atmosphere due to scattering and absorption by atmospheric gases, aerosol and clouds. The one dimensional radiative transfer is solved separately, once for the clear sky and once for the cloudy column which are subsequently combined according to cloud fraction. As the instantaneous distribution of clouds and water vapor are input to the radiation scheme, GHI reflects the strong dynamic variability of the atmosphere (Fig. 1).

The aerosol input to the radiation scheme is based on the Tanré et al. (1984) climatology and combines the effect of five different types of aerosols: continental, maritime, urban, volcanic and stratospheric background aerosols. The horizontal distribution of the aerosol types is based on the Global Aerosol Data Set (GADS, Koepke et al., 1997).

<sup>1</sup> <https://www.herz-tb4.uni-bonn.de>.

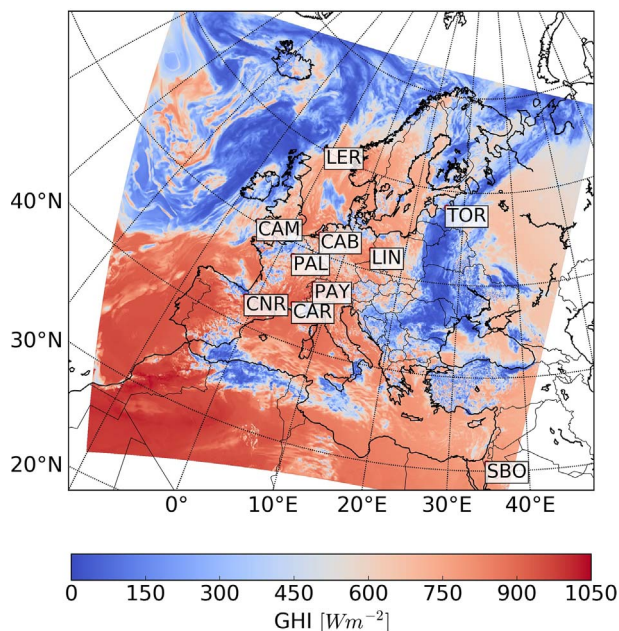


Fig. 1. Example of GHI field as provided by COSMO-REA6 for 12 UTC, 01 June 2014. The abbreviations show the considered Baseline Surface Radiation Network (BSRN) stations and their locations. The stations are geographically located at the upper left corner of the abbreviation box. The associated station names and coordinates can be found in Table 1.

Compared to other aerosol climatologies and observations, Zubler et al. (2011) showed that the Tanré climatology exhibits unrealistically high values of aerosol optical thickness for the European region (factor 2–3).

Despite the known disadvantages of the Tanré aerosol climatology it was used for the COSMO-reanalyses, as it is the standard input in the operational COSMO model setup at DWD. The aerosol climatology was not changed, as the COSMO model is known to provide good forecasts of e.g. precipitation, when using standard boundary fields. Nevertheless, within the framework of renewable energy research it might be advantageous to use a more realistic aerosol climatology, as already done in many other current NWP models.

Unless noted otherwise, we use the instantaneous output fields (every 15 min) of the short wave direct radiation  $Q_{dir}$  and the short wave diffuse radiation  $Q_{dif}$  at the surface from COSMO-REA6. The global horizontal irradiance  $Q_{GHI}$  is then obtained as

$$Q_{GHI} = Q_{dir} + Q_{dif} \quad (1)$$

by adding the direct and diffuse part of the short wave radiation at each grid point. Because GHI strongly depends on the solar elevation angle and thus on the diurnal and seasonal cycle, this dependency is eliminated by transforming GHI to transmissivity  $T$ , defined as

$$T = \frac{Q_{GHI}}{Q_{TOA}} \quad (2)$$

with  $Q_{TOA}$  the incoming irradiance at the Top Of the Atmosphere (TOA). The transmissivity is also called clearness index. Larger values refer to a clearer atmosphere, i.e. less radiation is extinguished mainly by aerosol and clouds. Considering transmissivity instead of GHI provides the benefit to be independent of the incoming TOA radiation amount. It should be noted that the ray path through the atmosphere is still a function of the solar elevation angle. Transmissivity is therefore positively correlated with this angle.

## 2.2. ERA-Interim

The global reanalysis ERA-Interim (Dee et al., 2011) provides data since 1979 to present. The hydrostatic model setup of ERA-Interim is based on the Integrated Forecasting System of the European Centre for

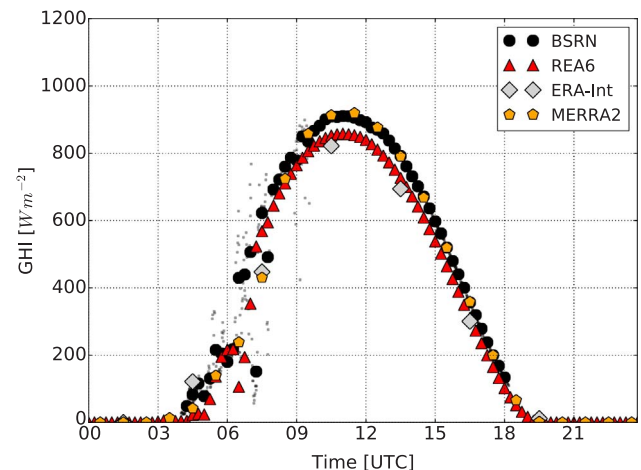


Fig. 2. Time series of GHI at Lindenberg, Germany, on June 23, 2008. BSRN measurements are given as 1 min averages (small dots) and 10 min averages (large black dots). COSMO-REA6 provides instantaneous values every 15 min (red), MERRA-2 every 1 h (orange), and ERA-Interim gives three hourly averages (grey). (For interpretation of the references to colour in this figure legend, the reader is referred to the web version of this article.)

Medium-Range Weather Forecasts (ECMWF) in the operational version of 2006 (IFS release Cy31r2). A four dimensional variational data assimilation scheme is applied for the assimilation of upper air variables, followed by separate schemes for near surface variables, soil moisture/temperature, snow and ocean waves. The 3D model fields are archived every 6 h at a horizontal resolution of approximately 80 km and 60 vertical levels. Two-dimensional fields are available every 3 h. For this study, we used the variable *Surface solar radiation downwards* with a temporal resolution of 3 h (<http://apps.ecmwf.int/datasets/data/interim-full-daily/>). ERA-Interim is frequently used for retrospective analysis in the meteorological community (e.g. Linares-Rodríguez et al., 2011; Ranjha et al., 2013). GHI fields from ERA-Interim are only available as three hourly averages and hence cannot resolve the variability due to clouds as is demonstrated in an example showing the diurnal cycle of GHI as obtained from ERA-Interim, COSMO-REA6, MERRA-2 and surface measurements (Fig. 2).

## 2.3. MERRA-2

The Modern-Era Retrospective Analysis for Research and Applications-2 (MERRA-2) is the latest global reanalyses produced by the NASA Global Modeling and Assimilation Office (GMAO, Molod et al., 2015). MERRA-2 is based on the Goddard Earth Observing System Model, Version 5 atmospheric general circulation model (AGCM). Observations are assimilated by the atmospheric data assimilation system (ADAS), version 5.12.4. MERRA-2 is the first global reanalyses assimilating space-based observations of aerosols (Randles et al., 2016).

MERRA-2 products are available since 1980 on a horizontal resolution of about 50 km in the latitudinal direction. For our study we use the global horizontal irradiation (name of variable: *surface\_incoming\_shortwave\_flux*) which is provided half past each hour (hourly resolution). All MERRA-2 data are freely accessible online through the NASA Goddard Earth Sciences Data Information Services Center (GES DISC).

## 2.4. Surface measurements

In order to assess the quality of the reanalyses, we use the freely available GHI measurements of the Baseline Surface Radiation Network (BSRN, Ohmura et al., 1998, <https://dataportal.pangaea.de/bsrn/>). The network was established in 1992 (Heimo et al., 1993) and contains

**Table 1**

GHI statistics before (COSMO-REA6) and after applying the post-processing (COSMO-REA6pp) for all considered BSRN stations. Years states the time range and Nobs the number of available measurements. The bias, the root mean square error (RMSE), bias corrected RMSE (BCRMSE), the mean absolute error (MAE), and the Pearson correlation (R) are based on the difference between modeled data and the BSRN measurements. The cross-validation results show the statistics when applying the post-processing to independent sites (see Section 5.3). The italic sites are rejected from the estimation procedure of the scaling factors (see Section 4).

Station name	Years	Nobs	COSMO-REA6 [ $\text{W m}^{-2}$ ]					COSMO-REA6pp [ $\text{W m}^{-2}$ ]				Cross-validation results [ $\text{W m}^{-2}$ ]			
			R	Bias	RMSE	BCRMSE	MAE	Bias	RMSE	BCRMSE	MAE	Bias	BCRMSE	MAE	
LIN	Lindenberg	95–09	202723	0.84	−2.9	129.8	129.7	87.4	5.2	136.6	136.5	86.9	5.4	136.6	87.0
CAM	Camborne	01–14	183926	0.81	2.2	142.8	142.8	100.0	11.8	152.8	152.3	103.3	12.1	152.6	103.6
CAR	Carpentras	96–14	253580	0.90	−29.8	122.2	118.5	86.1	−7.8	123.5	123.3	72.4	−9.8	123.0	72.8
CNR	Cener	09–14	76731	0.85	−19.6	144.9	143.5	100.9	−2.8	151.9	151.9	95.3	−3.1	151.9	95.3
CAB	Cabauw	05–14	134150	0.81	−18.4	138.8	137.5	94.6	−13.3	146.5	145.9	96.7	−14.2	146.2	97.0
PAL	Palaiseau	05–14	123935	0.81	−7.6	144.4	144.2	99.8	1.0	152.4	152.4	100.0	0.7	152.6	100.1
TOR	Toravere	99–14	163839	0.84	−8.2	121.3	121.0	81.1	1.5	126.8	126.7	79.5	2.0	126.8	79.6
PAY	Payerne	95–11	208568	0.86	10.4	134.6	134.2	93.3	22.8	139.5	137.6	87.2	24.3	137.4	87.5
Mean			1347452	0.84	−9.2	134.9	133.9	92.9	2.3	141.3	140.8	90.5	2.2	140.9	90.4
STD			1347452	0.03	12.1	8.9	9.4	6.9	10.6	10.9	10.9	9.9	11.4	11.0	9.9
<i>LER</i>	<i>Lerwick</i>	01–14	155356	0.75	12.6	136.3	135.7	97.9	18.5	147.1	145.9	102.5			
<i>SBO</i>	<i>Sede Boqer</i>	03–12	131584	0.94	−49.7	109.3	97.3	83.2	−14.4	103.3	102.3	59.4			

measurements from 1992 to the present. The BSRN network is chosen as it comprises high temporal resolution measurements over long periods with high data quality. According to (Gueymard and Myers, 2009) it is crucial to use only the highest quality data as those from the BSRN network, since other suboptimal data might result in an incorrect assessment. The measurement accuracy of BSRN GHI is estimated to be about  $5 \text{ W m}^{-2}$  (Ohmura et al., 1998). Altogether ten sites of the BSRN network are located in the COSMO-REA6 model domain (see Fig. 1 and Table 1) comprising different climate regimes within Europe.

The high quality of the BSRN measurements is achieved by applying strict quality control and quality assurance protocols (König-Langlo et al., 2013). In addition, (König-Langlo et al., 2013) recommend that every user should consider further quality control. Therefore, we applied tests provided by Long and Dutton (2002), namely the so-called “Extremely Rare Limits” tests, and two comparison tests to check the consistency of the three measurements: GHI, direct and diffuse radiation. The application of these quality control tests leads to a reduction in the number of measurements of about 2.6%. When comparing gridded reanalyses data with local measurements one has to consider that the reanalyses data provide quantities representing a relative large model grid box area. Measurements, on the other hand, are affected by the local environmental conditions such as land cover and topography. In order to match the one minute resolution BSRN data with the instantaneous values from a COSMO-REA6 grid box, we applied a 10 min average to the measurements with an averaging window centered around the COSMO-REA6 output time step. This is motivated by the fact that an air parcel with a typical horizontal wind speed of  $10 \text{ m s}^{-1}$  needs 10 min to cross a spatial distance of 6 km. Averages are only computed when all one minute values within a 10 min window are available and the corresponding solar elevation angles are larger than  $10^\circ$ .

In order to separate cloudy and cloud free conditions we use measurements of the ceilometer network<sup>2</sup> operated by DWD. In total 87 sites, so-called SYNOP stations, in Germany provide measurements of GHI as 10 min averages and cloud base height (CBH) derived from lidar ceilometers. CBH is given as the lowest cloud base height (observed every 15 s) within a 10 min interval. Note that according to this definition CBH does not need to persist over the 10 min interval, i.e. partly cloudy conditions are also included. In order to match the COSMO-REA6 instantaneous output we consider only two values per hour which are centered around the COSMO-REA6 output step (“quarter past” and

“quarter to”). Considered CBH measurements are from the years 2007–2013.

### 3. Assessment of COSMO-REA6 GHI

The ability of COSMO-REA6 to provide the realistic variability of GHI is qualitatively demonstrated by an arbitrarily selected time series of GHI on June 23, 2008 at the BSRN station Lindenberg, Germany (Fig. 2). The large scatter of the one minute resolution data indicates broken cloudiness with alternating cloudy and clear sky periods in the first half of the day while the smooth shape of the GHI during the rest of the day points to clear sky conditions. When the BSRN measurements are averaged to 10 min the variability due to changing cloud conditions is still visible and similar to the one of COSMO-REA6 for the corresponding grid box. MERRA-2 represents the observed GHI measurements well in the clear sky period, but cloud induced variability in the morning seems to be too smooth. With its three hour averages ERA-Interim is not capable to represent cloud induced short-term variations at all.

In order to quantitatively assess the quality of the COSMO-REA6 GHI the 10 min average measurements for all BSRN station between 1995 and 2014 are compared with the corresponding reanalysis data. The scatter density plot (Fig. 3) of more than 1.6 million matching pairs shows that most samples are clustered along the main diagonal indicating a good overall agreement with a mean difference between the reanalyses and measurements (bias) of  $-10 \text{ W m}^{-2}$  and a correlation coefficient of 0.86. The scatter density plot shows two distinct features: (1) Small observed GHI values are quite often overestimated by COSMO-REA6 and (2) GHI values higher than approx.  $1000 \text{ W m}^{-2}$  do not occur at all in COSMO-REA6 although these are represented in the measurements. Because such high values are related to cloud free situations with high solar elevation angle the underestimation in COSMO-REA6 indicates a too strong extinction of solar radiation likely caused by aerosols. This effect is even visible in the time series of a single day (Fig. 2). Given the small bias of  $-10 \text{ W m}^{-2}$  (averaged over the whole data), we hypothesize compensation effects of the two listed characteristics.

Table 1 provides a statistical comparison between instantaneous COSMO-REA6 GHI and measurements (10 min averages) for each BSRN site in terms of bias, RMSE, and the correlation coefficient. In order to support the following discussion of Table 1 in terms of cloud characteristics, transmissivity mean values and its variance are given in Table 2. The mean difference between the reanalyses and measurements (i.e., the bias) varies between  $-49.7 \text{ W m}^{-2}$  and  $12.6 \text{ W m}^{-2}$

<sup>2</sup> re3data.org; SAMD; editing status 2017-04-09; re3data.org Registry of Research Data Repositories, doi:10.17616/R3D944, 2017.

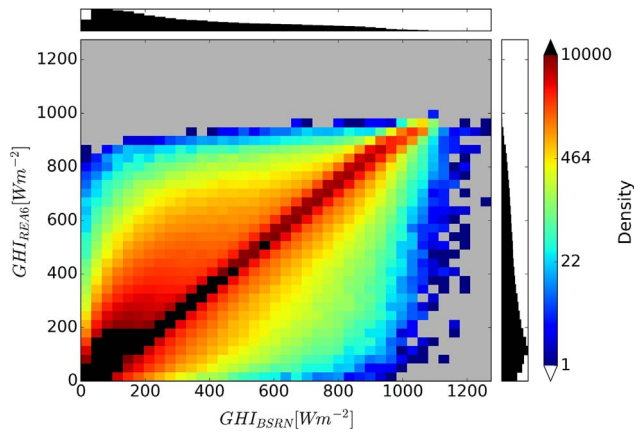


Fig. 3. Scatter density plot of GHI between measurements from all ten BSRN sites (10 min averages) and corresponding values from COSMO-REA6 (instantaneous). The time frame is 1995–2014.

among the sites (Table 1). The root mean square error (RMSE) values between 100 and 145  $W m^{-2}$  might appear high but are related to the high resolution providing realistic variations in GHI from COSMO-REA6 (Figs. 1 and 2). Therefore a slight misplacement of clouds in time or space will lead to strong differences compared with measurements. In order to compare the RMSE with those from global reanalysis daily GHI is assessed later on in Section 5.

From the list of stations, Sede Boqer (Israel) stands out, as it has a large negative bias ( $-49.7 W m^{-2}$ ) but shows the highest correlation with COSMO-REA6 of all sites. The high correlation and low RMSE is probably caused by the low average cloudiness at Sede Boqer (see Table 2, Sede Boqer has on average high transmissivity and low variance). As already discussed above the high cloud variability on small scales leads to a poor performance of the reanalysis when a slight shift of a cloud in time or space occurs. With respect to the negative bias, there are probably two causes: (1) Sede Boqer’s proximity to the border of the COSMO-REA6 domain with the resulting boundary effects, and (2) the low prevalence of clouds. The latter is consistent with the use of an optically too thick aerosol climatology in COSMO-REA6 (see Section 2) that results in a negative bias in clear sky situations due to too strong radiation attenuation by aerosols. At the site Lerwick, the largest positive bias of GHI ( $12.6 W m^{-2}$ ) occurs in combination with the smallest correlation coefficient (0.75). In contrast to Sede Boqer, Lerwick (Scotland) which shows the highest positive bias ( $12.6 W m^{-2}$ ) is situated close to the North Sea with high cloudiness i.e. the averaged transmissivity values are low (Table 2).

Table 2

Transmissivity characteristics of observations, COSMO-REA6, and the post-processed transmissivity product COSMO-REA6pp for each BSRN site. The underlying dataset is the same as used for Table 1, but transformed into transmissivity values.

		Transmissivity obs		COSMO-REA6		COSMO-REA6pp		Cross-validation results	
Station name		Mean	Var	Mean	Var	Mean	Var	Mean	Var
LIN	Lindenberg	0.43	0.054	0.42	0.039	0.43	0.054	0.43	0.054
CAM	Camborne	0.42	0.054	0.42	0.043	0.43	0.059	0.43	0.059
CAR	Carpentras	0.55	0.048	0.51	0.031	0.53	0.045	0.53	0.045
CNR	Cener	0.51	0.055	0.48	0.039	0.49	0.055	0.49	0.055
CAB	Cabauw	0.42	0.052	0.39	0.041	0.40	0.055	0.40	0.055
PAL	Palaiseau	0.44	0.054	0.43	0.040	0.43	0.055	0.43	0.055
TOR	Toravere	0.43	0.058	0.42	0.041	0.43	0.057	0.43	0.058
PAY	Payerne	0.44	0.060	0.46	0.036	0.47	0.052	0.47	0.052
Mean		0.46	0.054	0.44	0.039	0.45	0.054	0.45	0.054
STD		0.05	0.003	0.04	0.003	0.04	0.004	0.04	0.004
LER	Lerwick	0.37	0.052	0.39	0.042	0.40	0.057		
SBO	Sede Boqer	0.64	0.022	0.59	0.013	0.62	0.023		

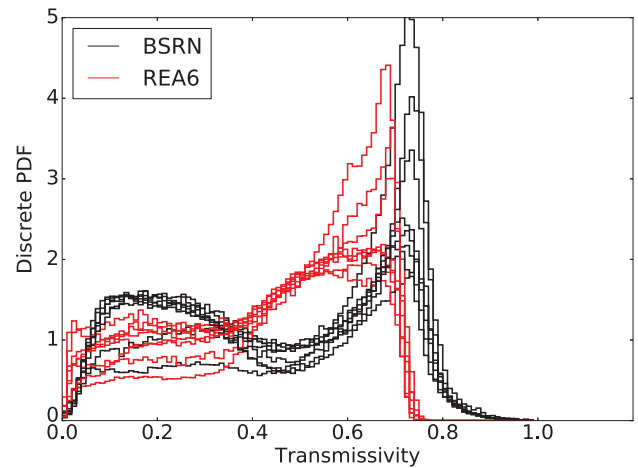


Fig. 4. Discrete Probability Density Functions (PDF) for transmissivity from BSRN measurements (black) and COSMO-REA6 (red). Each individual line represents a BSRN station. Lerwick and Sede Boqer are omitted here. The bin sizes are 0.01. (For interpretation of the references to colour in this figure legend, the reader is referred to the web version of this article.)

The apparent dependency of the bias on the cloud climatology motivates a refined analysis in respect to the effect of clouds on the extinction of solar radiation. For this purpose we look at the discrete probability density function for transmissivity  $T$  (Fig. 4) as defined in Section 2.1. For all BSRN stations the measurements reveal a bimodal distribution with local transmissivity maxima around 0.2 and 0.7. The high transmissivity maximum around 0.7 shows a more pronounced peak whose amplitude strongly varies between stations. As high transmissivity is typically associated with clear sky the amplitude of this peak likely reflects the differences in clear sky occurrence at the different sites. The broader low transmissivity peak around 0.2 is likely connected with cloudy conditions. Thus, we hypothesize that the local minimum around 0.5 separates cloudy from clear sky conditions which differs from the value of 0.7 given by Boilley and Wald (2015) for daily mean values.

In order to test our hypotheses the SYNOP data set (Section 2.4) with corresponding GHI and ceilometer measurements for Germany is used. When looking at the observed Probability Density Function (PDF) of transmissivity (Fig. 5) a similar bimodal distribution as for the BSRN station appears. The ceilometer measurements allow to stratify the data into different cloud conditions which confirms that the majority of high transmissivity cases originates from clear sky conditions. Also high clouds defined as clouds with a base of 5 km and higher are mostly

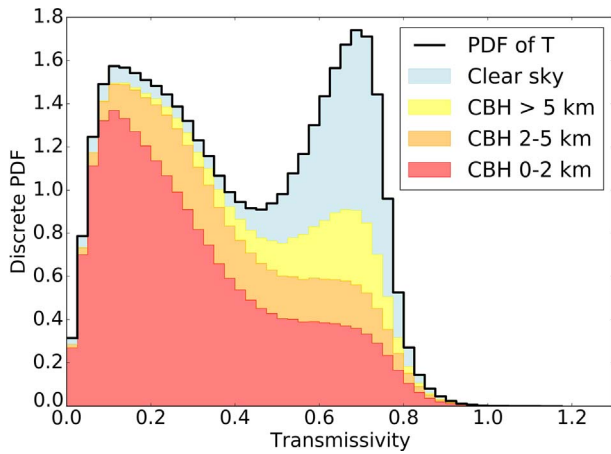


Fig. 5. Discrete probability density function for transmissivity measured at 87 German SYNOP stations with corresponding ceilometer measurements. Colors indicate the cloud situation as given by the ceilometer measurements: Clear sky conditions (blue), high clouds (yellow), medium altitudes (orange) and low level clouds (red). See text for definitions. (For interpretation of the references to colour in this figure legend, the reader is referred to the web version of this article.)

associated with high transmissivities. These are commonly composed of ice particles and show a much lower average optical depth explaining their high transmissivity. Lower transmissivities mostly comprise cases with low (cloud base below 2 km) and medium high (cloud base between 2 and 5 km) clouds. Only a few high transmissivity cases with low or medium CBH exist. These can be explained by the fact that even the appearance of one 15 s cloudy sample within 10 min will still lead to the measurement of a CBH although the majority of time is cloud free. Furthermore, the ceilometer measures only vertically while GHI measurements are influenced by the whole hemisphere. The difference in sampling may lead to the determination of clear sky conditions from ceilometer measurements in a nearly overcast sky and vice versa.

The frequency distribution of COSMO-REA6 transmissivity (Fig. 4) shows some differences compared to the measurements. As already seen in the scatter density plot (Fig. 3) highly transparent scenes with transmissivities higher than 0.8 do not appear and the whole distribution seems to be squeezed towards lower transmissivities compared to the measurements. Nevertheless, the strong variability in amplitude of the high transmissivity peak is reproduced indicating that the reanalysis is able to represent the cloud climatology (true/false events) at the different sites. For transmissivities in the medium range many more cases compared to measurements occur indicating that clouds are optically relatively thin in COSMO-REA6. The narrower transmissivity distribution is in accordance with the systematic underestimation of transmissivity variance by COSMO-REA6 as shown in Table 2. In summary, two different characteristics in COSMO-REA6 appear: (1) GHI is underestimated in clear sky conditions due to the use of the Tanré aerosol climatology which is known to exhibit unrealistically high values of aerosol optical thickness (Zubler et al., 2011) and (2) on average, clouds are optically too thin causing an overestimation of GHI.

#### 4. GHI post-processing

Given the under- and overestimation of GHI as described in the previous section we developed a post-processing using reanalysis data only to correct the systematic differences for the clear sky and the cloudy regime, separately. The proposed post-processing is based on the determination of scaling factors for GHI from COSMO-REA6 through orthogonal distance regression (ODR, described in detail by [under the name total least-squares method] Markovsky and Huffel, 2007) using different scaling factors for either cloudy or clear sky situations. A transmissivity threshold  $T_{th}$  is used to distinguish both regimes.  $T \geq T_{th}$  refers to clear sky and  $T < T_{th}$  refers to cloudy sky (see Section 3).

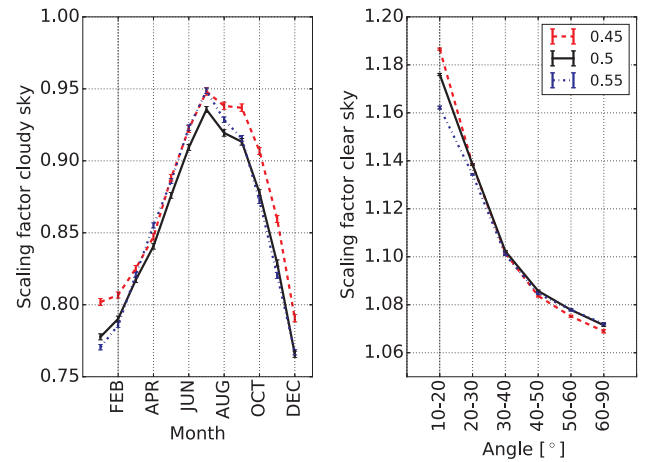


Fig. 6. Sensitivity of the estimated scaling factors to transmissivity thresholds  $T_{th}$  for the cloudy regime with low transmissivity values ( $T < T_{th}$ , left) and the clear sky regime with high transmissivity values ( $T > T_{th}$ , right). Different colors represent the scaling factors estimated with  $T_{th} = 0.45$  (red),  $T_{th} = 0.5$  (black), and  $T_{th} = 0.55$  (blue). Vertical lines illustrate the uncertainties of the ODR fit. (For interpretation of the references to colour in this figure legend, the reader is referred to the web version of this article.)

Furthermore, we consider the annual cycle and the solar elevation angle which describes the length of the light path in the atmosphere as potential influence factors for the under- or overestimation of GHI. Therefore, the scaling factor  $a$  generally depends on the predictor  $T$  as well as on the month of year  $m$  and the solar elevation angle  $\theta$ :

$$a(T, m, \theta) = \begin{cases} a_{\text{clear}, \theta} & \text{for } T \geq T_{th} \\ a_{\text{cloud}, m} & \text{for } T < T_{th} \end{cases}$$

with  $a_{\text{clear}, \theta}, a_{\text{cloud}, m}$  the scaling factors for clear sky and cloudy conditions, respectively. The post-processed GHI ( $Q_{GHIpp}$ ) is then defined as

$$Q_{GHIpp} = Q_{GHI} \cdot a(T, m, \theta) \quad (3)$$

with  $Q_{GHI}$  being the global horizontal irradiance of the reanalysis. Using the TOA radiation  $Q_{TOA}$ , Eq. (3) can be easily transformed to the transmissivity space ( $T = \frac{Q_{GHI}}{Q_{TOA}}$ ) as:

$$T_{pp} = T \cdot a(T, m, \theta) \quad (4)$$

with  $T_{pp}$  the post-processed transmissivity and  $a(T, m, \theta)$  the invariant scaling factors from Eq. (3).

The scaling factor  $a(T, m, \theta)$  is determined as the slope of the linear ODR between the BSRN- and the COSMO-REA6 transmissivity. The ODR has the advantage to consider uncertainties in both, measurements and reanalyses. The best case ODR would have a slope equal to the angle bisector ( $a = 1$ ), thus no adjustment would take place. It should be mentioned that the ODR regression is forced to cross the coordinate origin to keep very small radiation values unchanged, otherwise the ODR would in some cases generate negative radiation values. For cloudy situations twelve scaling factors are estimated, one for each month. For clear sky situations six scaling factors are estimated, one for each solar elevation regime: 10°–20°, 20°–30°, 30°–40°, 40°–50°, 50°–60° and 60°–90°.

In general, the scaling factors are determined by the annual cycle of the cloud- and aerosol climatologies as well as by the solar elevation angle. In both regimes (clear and cloudy) all of these dependencies are directly or indirectly considered. For simplicity we only consider the seasonal variation under cloudy sky conditions ( $a_{\text{cloud}, \theta}$ ) due to the dominance of diffuse radiation over direct radiation. Under clear sky conditions ( $a_{\text{clear}, m}$ ) the sun position is more important since aerosol (and water vapor) extinction, which depends mainly on the path of direct solar radiation, dominates.

The scaling factors  $a(T, m, \theta)$  are determined from all available matches of reanalyses data and measurements from eight BSRN sites in

Central and Western Europe (Table 1). The two stations with the minimum and maximum bias, i.e., Sede Boqer and Lerwick, are excluded. The transmissivity threshold distinguishing the clear sky and cloudy sky regimes has been set ad hoc to  $T_{th} = 0.5$ . Therefore the sensitivity of the estimated scaling factors to this threshold is investigated in more detail (Fig. 6). In the cloudy sky regime ( $T < T_{th}$ ) the estimated scaling factors are smaller than one because COSMO-REA6 overestimates the GHI compared to the measurements, i.e. the clouds are optically too thin. This effect can be seen during the whole year, but the effect is stronger for winter months with scaling factors around 0.8 than for summer with scaling factors around 0.93. When varying  $T_{th} = 0.5$  by  $\pm 10\%$  the scaling factor only changes by roughly  $\pm 2\%$ . Note: The scaling factors from March till September are smallest (largest adaptations necessary) for  $T_{th} = 0.5$ . Thus, the threshold  $T_{th} = 0.5$  is well chosen because an increase of  $T_{th}$  seems to include cases which need positive adjustments (cases of the clear sky regime), and a decrease of  $T_{th}$  seems to exclude cases which need negative adjustments (cases of cloudy sky regime). For clear sky conditions ( $T > T_{th}$ ) the scaling factor varies with the solar elevation angle between 1.19 for low and 1.07 for high solar elevation angles. A scaling factor larger than one indicates a general underestimation of the GHI by the reanalysis for these situations as already discussed in Section 3. The sensitivity of the scaling factor to the transmissivity threshold in this regime is highest for low elevation angles ( $< 20^\circ$  with values varying between 1.16 and 1.19) and nearly diminishes for medium elevation angles. In summary, the sensitivity to the transmissivity threshold seems to be marginal. Therefore, the chosen threshold value of  $T_{th} = 0.5$  is used for the post-processing approach.

In order to combine the clear sky and cloud regime, post-processing such that a continuously distributed transmissivity without a discontinuity at the transmissivity threshold  $T_{th}$  is achieved, a weight function is applied. A sigmoid function is chosen as weighting function, which is defined as

$$f = \frac{1}{1 + \exp\left(-\frac{1}{c}(x-b)\right)} \quad (5)$$

with the coefficient  $b$  shifting the function on the x-axis and the coefficient  $c$  defining the slope of the sigmoid function. In our application, the coefficient  $b$  is set to the transmissivity threshold which distinguishes between the two regimes ( $b = T_{th} = 0.5$ ). The slope of the sigmoid function  $c$  is estimated in order to minimize the distance between the observed and post-processed discrete PDF over all eight BSRN stations. The quantity measuring the distance between two probability distributions is known as Earth Mover's Distance (EMD, Rabin et al., 2008). By minimizing EMD an optimum slope of  $c = 0.03$  is derived which results in an EMD improvement of factor 4 compared to the EMD before post-processing (not shown).

## 5. Evaluation of the new GHI data set

The post-processing described in Section 4 is applied to the COSMO-REA6 reanalysis. To reduce computational costs, the solar position was calculated for every third grid point and was afterwards linearly interpolated to the complete model grid. The post-processed GHI data set covers the time period from January 1, 1995 to December 31, 2014 with a temporal resolution of 15 min for  $848 \times 824$  grid points in the European domain (Fig. 1). The resulting post-processed product of COSMO-REA6 GHI is from now on referred to as COSMO-REA6pp.

### 5.1. Marginal distribution

In order to test the quality of the post-processing, Fig. 7 shows the deviation of the transmissivity distribution to the measured one for both COSMO-REA6 and COSMO-REA6pp. The figure clearly shows that the under- and overestimation identified in Fig. 4 have been

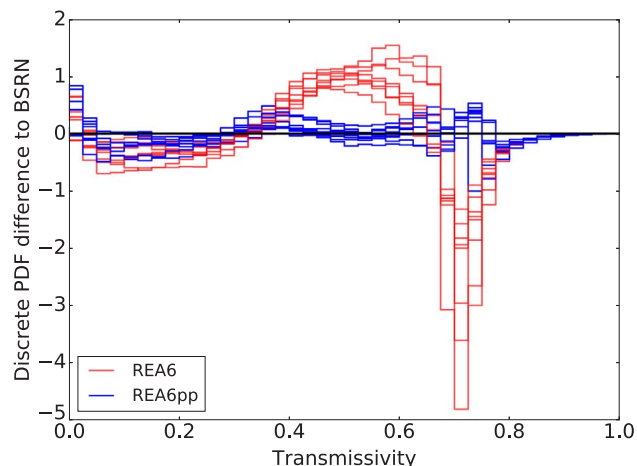


Fig. 7. Difference between the transmissivity distribution from measurements and the one from COSMO-REA6 (red) and COSMO-REA6pp (blue). Sites used for estimating the scaling factors are considered only. Positive values indicate an overestimation of COSMO-REA6 while negative values show an underestimation. (For interpretation of the references to colour in this figure legend, the reader is referred to the web version of this article.)

significantly reduced for all transmissivities: (i) The clear sky peak of COSMO-REA6 as a consequence of the strong aerosol extinction has now been shifted to transmissivities around 0.8 much closer to the observed values. (ii) The underestimation of transmissivities below 0.4 associated with too thin clouds has been eliminated. An equivalent illustration of the bias reduction depending on transmissivity is given by Fig. 8.

#### 5.1.1. Separate evaluation for clear sky and cloudy conditions

The post-processing has mainly been developed in order to reduce the systematic bias in “clear sky” ( $T > T_{th}$ ) and “cloudy sky” ( $T < T_{th}$ ) situations. Since the method is not designed to handle the problem of misrepresented clouds in COSMO-REA6, only situations where both transmissivity values – observed and reanalyzed – simultaneously lie above or under the threshold, are considered in the evaluation of GHI (Fig. 9).

For each BSRN site the monthly mean bias in COSMO-REA6 (dashed) and COSMO-REA6pp (solid) is evaluated. In case of clear sky situations, an improvement is evident for all individual sites (Fig. 9a). The general underestimation of GHI in COSMO-REA6 with bias values between  $-62$  and  $-30 \text{ W m}^{-2}$  depending mainly on the site has

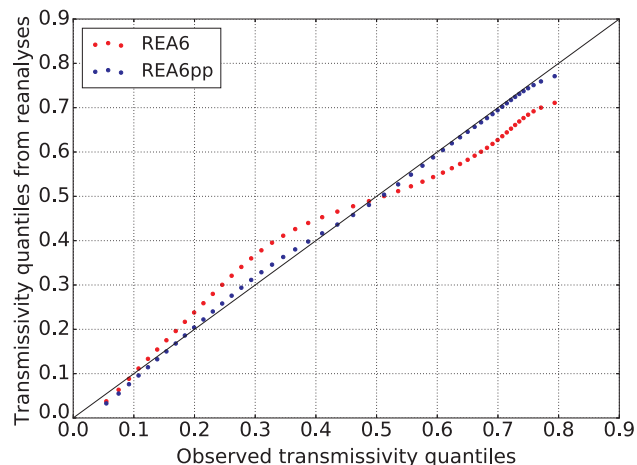


Fig. 8. Quantile-quantile plot comparing the transmissivity distribution from measurements and the one from COSMO-REA6 and COSMO-REA6pp. Considered observations are from the eight BSRN stations listed in Table 1.

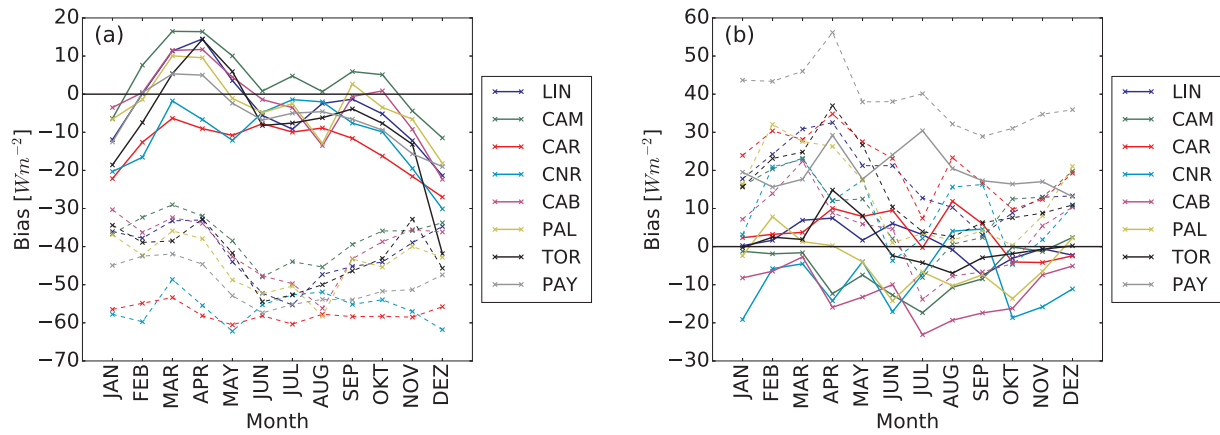


Fig. 9. Monthly mean bias for COSMO-REA6 (dashed) and COSMO-REA6pp (solid lines) for (a) clear sky situations and (b) cloudy sky situations. To calculate the monthly averages, we considered only situations where the observed transmissivity and the COSMO-REA6 transmissivity simultaneously exceeds 0.5 (a) or is below 0.5 (b).

disappeared in COSMO-REA6pp with most monthly mean values between  $-20$  and  $20 \text{ W m}^{-2}$ . Nevertheless, a systematic (but reduced) underestimation remains during the winter months, particularly in December. This is probably caused by the annual cycle of clear sky ( $T \geq T_{th}$ ) and cloudy sky ( $T < T_{th}$ ) situations with  $\sim 32\%$  ( $\sim 55\%$ ) of cases being clear sky situations in winter (summer) months. Local effects could also be responsible for the worst bias of  $-40 \text{ W m}^{-2}$  in Toravere, Estland, in December.

The bias has also been improved in COSMO-REA6pp for cloudy sky situations (Fig. 9b). While the bias before the post-processing ranges from  $-18 \text{ W m}^{-2}$  to  $59 \text{ W m}^{-2}$ , afterwards it is reduced to values ranging from  $-22 \text{ W m}^{-2}$  to  $38 \text{ W m}^{-2}$ . Nevertheless, some sites still exhibit a systematic positive or negative bias which are caused by local effects.

### 5.2. Joint distribution

To assess the improvements of the post-processing at individual times and locations, Table 1 compares bias, RMSE, bias corrected RMSE (BCRMSE), and mean absolute error at individual stations before and after post-processing (COSMO-REA6pp). The usage of the two sites that have not been used in the estimation of the post-processing parameters (Sede Boquer and Lerwick colored in red) allows for a performance assessment of the post-processing method for independent measurements. After post-processing, the large bias at most stations including Sede Boquer is significantly reduced, e.g. the bias is reduced from  $-29.8$  to  $-7.8$  at Carpentras, France, and from  $-19.6$  to  $-2.8 \text{ W m}^{-2}$  at Cener,

Spain. This reduction is expected as sites with large biases are mostly effected by one of the two regimes. The RMSE and the BCRMSE, which are sensitive to departures in the tails of the distribution, show slightly increased values. Considering that the post-processing increases the number of low as well as high radiation cases, it broadens the distribution function of the GHI. Since the largest deviations of the re-analysis from the measurements are caused by misrepresented clouds, the number of cases with large transmissivity deviations is increased. Thus, the RMSE and the BCRMSE, which weight deviations quadratically increase. In comparison, the MAE which weights all deviations to measurements equally shows an improvement (in seven of ten cases) of the post-processed radiation. The post-processing is derived from eight BSRN stations but applied to the full COSMO-REA6 domain. Therefore the application of the post-processing to the two independent test sites is most interesting. Here the MAE improves strongly from  $83.2$  to  $59.4 \text{ W m}^{-2}$  for Sede Boquer and becomes slightly worse ( $97.9$ – $105.2 \text{ W m}^{-2}$ ) for Lerwick.

As mentioned before, the post-processing leads to a broadening of the GHI/Transmissivity distribution. In order to check if that results in a more realistic distribution, the variance of observations, COSMO-REA6, and COSMO-REA6pp (after post-processing) are shown in Table 2. While COSMO-REA6 significantly underestimates the observed transmissivity variance, it is well represented by COSMO-REA6pp, even at the sites with different climatic conditions (Lerwick and Sede Boquer). Note that the mean values are more or less unchanged by the post-processing.

So far, the previous tables only showed the statistical results for all

Table 3  
Same as Table 1 but for clear sky situations only (both transmissivity values - observed and reanalyzed - are simultaneously above the threshold  $T_{th} = 0.5$ ).

	Station name	Years	COSMO-REA6 [ $\text{W m}^{-2}$ ]		COSMO-REA6pp [ $\text{W m}^{-2}$ ]		Cross-validation results [ $\text{W m}^{-2}$ ]		
			Bias	MAE	Bias	MAE	Bias	MAE	
	LIN	Lindenberg	63805	-43.8	59.0	-0.1	45.8	0.4	45.9
	CAM	Camborne	54025	-39.0	62.6	6.1	54.9	7.2	55.2
	CAR	Carpentras	140587	-57.9	65.8	-11.7	34.5	-14.6	35.6
	CNR	Cener	34097	-54.9	67.4	-7.7	42.8	-8.0	42.9
	CAB	Cabauw	36861	-42.2	58.7	0.8	49.1	0.9	49.3
	PAL	Palaiseau	39336	-45.8	62.3	-1.1	48.1	-0.9	48.2
	TOR	Toravere	54313	-44.5	53.2	-0.3	39.5	0.3	39.6
	PAY	Payerne	76618	-50.9	59.9	-3.6	37.3	-3.3	37.2
	Mean	Mean	499642	-47.4	61.1	-2.2	44.0	-2.2	44.2
	STD	STD	499642	6.1	4.2	5.1	6.3	6.1	6.2
	LER	Lerwick	155356	-40.2	63.8	2.9	56.9		
	SBO	Sede Boquer	131584	-67.8	75.2	-17.9	37.4		

**Table 4**Same as Table 1 but for cloudy sky situations only (both transmissivity values - observed and reanalyzed - are simultaneously below the threshold  $T_{th} = 0.5$ ).

	Station name	Years	COSMO-REA6 [ $Wm^{-2}$ ]		COSMO-REA6pp [ $Wm^{-2}$ ]		Cross-validation results [ $Wm^{-2}$ ]	
			Bias	MAE	Bias	MAE	Bias	MAE
LIN	Lindenberg	93451	17.6	63.0	1.4	58.6	1.3	58.6
CAM	Camborne	82716	8.8	73.3	-7.2	69.7	-7.5	69.7
CAR	Carpentras	59152	21.6	69.7	3.5	64.5	3.2	64.3
CNR	Cener	24411	9.2	75.8	-9.8	72.1	-10.1	72.1
CAB	Cabauw	64600	2.7	68.8	-12.9	66.4	-14.2	66.3
PAL	Palaiseau	53867	12.5	73.2	-5.0	68.9	-5.5	68.9
TOR	Toravere	75083	14.6	60.2	0.6	56.2	0.9	56.3
PAY	Payerne	85265	39.1	73.5	20.0	64.9	22.6	66.0
Mean	Mean	538545	15.8	69.7	-1.2	65.2	-1.1	65.3
STD	STD	538545	10.3	5.2	9.6	5.1	10.6	5.1
LER	Lerwick	155356	13.5	66.6	-0.1	63.1		
SBO	Sede Boqer	131584	8.1	44.1	-10.9	45.6		

data, i.e. they do not show the individual improvement for the cloudy and clear sky cases, separately. In order to investigate the improvement of the post-processing without bias compensation effects from the two cloud regimes, Tables 3 and 4 show the statistical results for clear and cloudy cases separately. The separation of “clear” and “cloudy sky” is done with the same criteria used for Fig. 9. In clear sky cases, there is an improvement in each individual score. The post-processing reduces the systematic biases of  $-39$  till  $-67.8 W m^{-2}$  to a range of  $-17.9$  till  $6.1 W m^{-2}$ . The MAE improves by at least 6.9 up to  $61.6 W m^{-2}$ . Also the RMSE improved for each individual site (not shown). In cloudy sky cases the bias improves at 7 of 10 BSRN stations. At the other 3 stations an over-adjustment took place. Nevertheless, the MAE improves at 9 of 10 stations, and the RMSE at all considered stations (not shown).

### 5.3. Cross-validation of the new GHI data set

Cross-validation is a common method to investigate the potential to generalize the application of a statistical method. The principle of cross-validation is to (1) divide the data into a training and verification data set, (2) estimate the statistical model using the training data, and (3) test the model with the verification data set (for more details see Storch and Zwiers, 2003; Stone, 1974; Michaelsen, 1987; Kohavi, 1995). In order to test the potential to spatially generalize the post-processing, cross-validation is applied by removing one observational site at time from the training data set while applying the approach. The last columns in Table 1 show the bias, BCRMSE and the MAE for the individual sites, by omitting the site while estimating the scaling factors. In comparison to the post-processed results using the full data set, the bias is slightly increased by 0.2 till  $1.5 W m^{-2}$  for all stations except for Palaiseau where the bias actually becomes smaller. However, all changes lie below the measurement uncertainty of  $5 W m^{-2}$  and no considerable changes can be found for BCRMSE and MAE. Also, when applying cross-validation to the clear and cloudy sky cases separately, the resulting scores are not significantly reduced compared to the COSMO-REA6pp scores (see Tables 3 and 4). Additionally, also the transmissivity variances changes just slightly comparing the cross-validation results with the dependent COSMO-REA6pp results (Table 2). Thus, it is expected that the developed post-processing produces improved radiation fields for the whole COSMO-REA6 model domain.

### 5.4. Daily mean values

Up to now we only considered instantaneous GHI values which are available at 15 min resolution from COSMO-REA6. Because of the coarser resolution of other reanalyses products, most previous studies (e.g. Boilley and Wald, 2015; Posselt et al., 2012) have been concerned

with daily mean values of GHI. In order to relate the performance of COSMO-REA6 to these studies in the following we compare the daily average GHI from COSMO-REA6 and COSMO-REA6pp to the global, coarser resolution ERA-Interim reanalysis using BSRN measurements as a reference. Note, that due to the quality control of BSRN measurements (Section 2.4) only the GHI values associated with solar angles greater than  $10^\circ$  are used to calculate the daily averages. For consistency COSMO-REA6 and COSMO-REA6pp have been treated similarly. However, the ERA-Interim 3-hourly data comprise also the radiation values of solar angles below  $10^\circ$ , thus causing a systematic error in the evaluation. This systematic difference in daily GHI due to the limitation in solar angles is estimated with the help of the continuous COSMO-REA6 data. Neglecting the low elevation angles leads to an underestimation of the daily average GHI of about  $2.9 W m^{-2}$  which needs to be kept in mind when interpreting the following results.

The statistical comparison of daily mean GHI from reanalysis with the ten BSRN stations is provided in the form of box-whisker diagrams in Fig. 10. The results indicate that COSMO-REA6 as well as COSMO-REA6pp are in better agreement with the observed GHI compared to ERA-Interim and MERRA-2, i.e. showing lower bias, RMSE and MAE as well as a higher correlation with measurements in the median of all

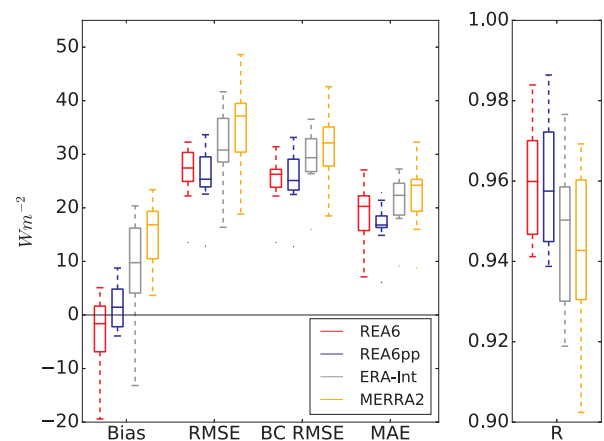


Fig. 10. Statistical assessment of daily mean GHI from COSMO-REA6, COSMO-REA6pp, ERA-Interim, and MERRA-2 over the years 1995–2014. The reference GHI is provided by the ten BSRN stations listed in Table 1. Each boxplot is created by 10 values, one for each BSRN site. The box extends from the first to the third quartile (interquartile range IQR) with a line at the median. The whiskers have the maximum length of 1.5 times IQR. All points beyond the whiskers (flyers) are shown as dots. Note that due to the consideration of sun elevation angles below  $10^\circ$  ERA-Interim is about  $2.6 W m^{-2}$  higher than all other data sets.

stations. As to be expected COSMO-REA6pp performs better compared to COSMO-REA6 in terms of bias and the MAE. For the latter the median improved from  $20.3 \text{ W m}^{-2}$  to  $16.8 \text{ W m}^{-2}$ . The benefit of the post-processing is most pronounced in the reduced length of whiskers for bias and MAE of COSMO-REA6pp meaning that systematic deficits at some of the stations could be cured without compromising the quality at other stations.

#### 5.4.1. Comparison to previous studies

Boilley and Wald (2015) evaluated two global reanalyses, i.e. ERA-Interim and MERRA as well as the HelioClim (Blanc et al., 2011) satellite product to GHI surface observations in different regions of the globe. They find a lower uncertainty in the satellite product and conclude that this should be preferred over the global reanalyses. Thus, the question arises whether COSMO-REA6pp which has shown improved performance compared to ERA-Interim has a similar quality as satellite products.

Posselt et al. (2012) investigated the performance of a variety of satellite and reanalysis GHI products using BSRN stations as reference. Because they included five additional BSRN stations outside the COSMO-REA6 domain their results are expected to be slightly different than ours. For ERA-Interim they found a daily mean bias of  $5.6 \text{ W m}^{-2}$  and a MAE of  $26.9 \text{ W m}^{-2}$  which are quite similar to our findings, i.e.  $6.6 \text{ W m}^{-2}$  (bias) and  $20.8 \text{ W m}^{-2}$  (MAE) where a correction for the solar elevation angle cutoff has been applied to the data from Fig. 10. This similarity for ERA-Interim encourages us to indirectly relate the performance of COSMO-REA6pp to the other products investigated by Posselt et al. (2012). Their best product, i.e. the satellite based product SARAH (Müller et al., 2015), reveals a similar performance (bias =  $4.6 \text{ W m}^{-2}$ , MAE =  $15.5 \text{ W m}^{-2}$ ) compared to COSMO-REA6pp in our study (bias =  $1.8 \text{ W m}^{-2}$ , MAE =  $16.8 \text{ W m}^{-2}$ ). All other products including HelioClim show a worse performance in representing measured daily GHI than COSMO-REA6pp.

#### 5.5. Spatio-temporal representation

One expected advantage of COSMO-REA6 compared to global reanalysis is the enhanced representation of observed GHI spatio-temporal variability. In order to confirm this, we apply the evaluation method proposed by Cannon et al. (2014) developed to assess the ability of a reanalysis to represent wind speed on different spatial scales. They calculate the linear correlation between measurements and reanalysis for wind speed differences at two geographically distant sites. By looking at the correlation as a function of site-to-site distance they evaluate on which scales the wind speed variability given by reanalysis is similar to the observed one. Here we apply the same method to GHI which has to our best knowledge not been done before. The method includes the following steps:

- Calculate the difference in GHI  $\delta Q$  between two sites  $i$  and  $j$  for measurements and reanalysis data, respectively

$$\delta Q_{obs} = Q_{obs,i} - Q_{obs,j} \quad (6)$$

$$\delta Q_{rea} = Q_{rea,i} - Q_{rea,j} \quad (7)$$

with  $Q = (Q_{t1}, \dots, Q_{tn})^T$

- Calculate the correlation:  $r(\delta Q_{rea}, \delta Q_{obs})$
- Do this calculation for every site combination
- Plot the results as function of distance between the observation sites

The linear correlation is derived for a data set from 119 German SYNOP stations available from 2007–2013 and is shown as a function of distance between stations in Fig. 11. We restrict the evaluation to the 9–12 UTC averages (1) to avoid issues with respect to the daily cycle inducing a positive correlation and (2) to match the ERA-Interim output

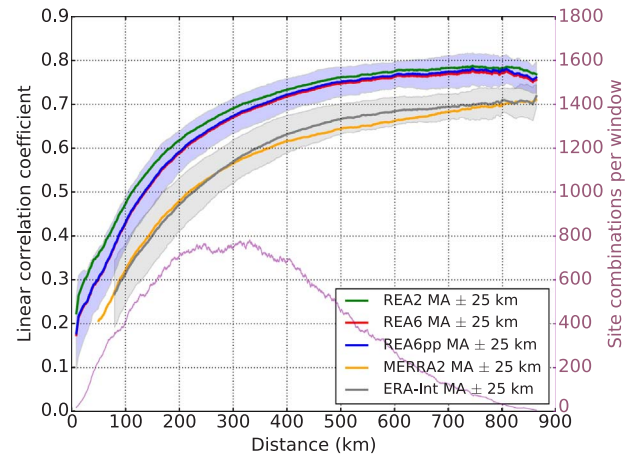


Fig. 11. Linear correlation of site to site GHI differences in model and corresponding differences in measurements as function of distance. The correlations between measurements and model are done for the models ERA-Interim (grey), MERRA-2 (orange), COSMO-REA6 (red), COSMO-REA6pp (blue), and COSMO-REA2 (green). The correlations are shown as moving averages about  $\pm 25 \text{ km}$ . Shaded is the standard deviations of all correlations in the considered moving window (shown for ERA-Interim and COSMO-REA6pp). The magenta line shows the number of correlation values per moving average window. (For interpretation of the references to colour in this figure legend, the reader is referred to the web version of this article.)

interval. In general the correlation increases steadily with increasing distance and starts to level off around 300–500 km distance. The general evolution from smaller to larger correlation with increasing distance is caused by the better representation of large scales, e.g. frontal systems, compared to small scale phenomena in numerical weather prediction models. For COSMO-REA6, the low correlation of less than 0.3 for scales below 50 km is due to small scale clouds. These are frequently related to convection at sub-grid scales making it very difficult to simulate clouds exactly at the correct spatio-temporal location. By averaging over larger areas or time intervals this uncertainty is effectively reduced as can be seen in the strong reduction of the MAE from roughly  $100 \text{ W m}^{-2}$  (Table 1) for instantaneous GHI compared to  $20 \text{ W m}^{-2}$  (Fig. 10) for daily means.

While ERA-Interim, MERRA-2, and COSMO-REA6 show a similar shape of the linear correlation as a function of distance COSMO-REA6 outperforms both global reanalyses with a higher correlation at all scales (Fig. 10). Comparing the two global reanalyses, ERA-Interim performs slightly better on scales above 270 km. The maximum correlation is 0.7 for both global reanalyses and 0.8 for COSMO-REA6. As expected the post-processing does not influence the resolved variability and COSMO-REA6pp is nearly identical to COSMO-REA6. The advantage of the high resolution reanalysis is especially visible at shorter scale, i.e. at 100 km the correlation is about 0.3 for both global reanalyses while it is 0.42 for COSMO-REA6. To investigate whether an even higher resolution improves the representation of small scale clouds even further, we also investigate the performance of the convection-permitting 2 km reanalysis COSMO-REA2 available only for Germany. The comparison (Fig. 10) clearly shows that COSMO-REA2 represents the observed GHI variability best for all scales and especially at small scales reaching a correlation of 0.47 at 100 km distance. In summary, both COSMO reanalyses are able to represent spatio-temporal distributions of GHI significantly better than ERA-INTERIM and MERRA-2. Thus, also cloud distributions and the connected atmospheric processes are more realistically represented in the high resolution reanalyses.

#### 5.6. Ramp rates

Ramp rates, i.e. the temporal variability of transmissivity, are most important for the solar energy sector. Extreme ramp rates cause fast

changes of power production and might be critical for grid stability. Thus, we want to investigate whether ramp rates obtained from COSMO-REA6 and COSMO-REA2 are statistically consistent with the observed ones.

NWP models and reanalyses are known to have deficits in representing clouds at the exact spatio-temporal location. Furthermore, the coarse spatial resolution smoothes the representation of short term characteristics. Nevertheless, the statistics of the variability should match at least on the temporal scales greater than the effective resolution of the reanalyses. To test the performance of representing ramps, we use the cumulative distribution function (CDF) of

transmissivity ramp rates ( $\Delta T$ ). Using CDFs is reasonable, as the ramps do not need to occur at the same spatio-temporal location. Nevertheless, it shows whether ramps are statistically represented with the correct intensity.

The CDFs of  $\Delta T$  are generated for temporal resolutions (a) 3 h, (b) 1 h, and (c) 30 min (Fig. 12). The ramp rates in case (a) are the differences of the 3 h average from 9–12 and 12–15 UTC. In case (b) and (c) the ramp rates are based on the hourly and 30 min averages of each day in 2007–2013 between 11 and 14 UTC, respectively. Average values from the COSMO reanalyses are approximated by averaging instantaneous values given all 15 min i.e. four instantaneous values represent one hour. In case of MERRA-2 instantaneous values given all 60 min are used to calculate the aimed averaging interval. From Fig. 12 it is evident that observed ramps on a three hour scale are best represented by COSMO-REA6pp, ERA-INT, MERRA-2, COSMO-REA6, and COSMO-REA2 underestimate extreme ramp rates, i.e. the most extreme upper 10% of observed ramp rates are underestimated by about 50%. MERRA-2 performs best when comparing with the other original reanalysis products. The CDFs for the higher temporal resolutions show in general the expected reduction of the reanalyses ability to represent extreme ramp rates (smoothing effect). Considering one hour ramp rates, the regional reanalyses perform better than MERRA-2, indicating a more pronounced smoothing effect for the global product. While the COSMO-REA6pp CDF is still close to the observed one for a time scale of one hour, the ramp rates are underestimated considerably for time scales of 30 min i.e. the upper 10% of observed ramp rates are underestimated by about 1% and 30%, respectively.

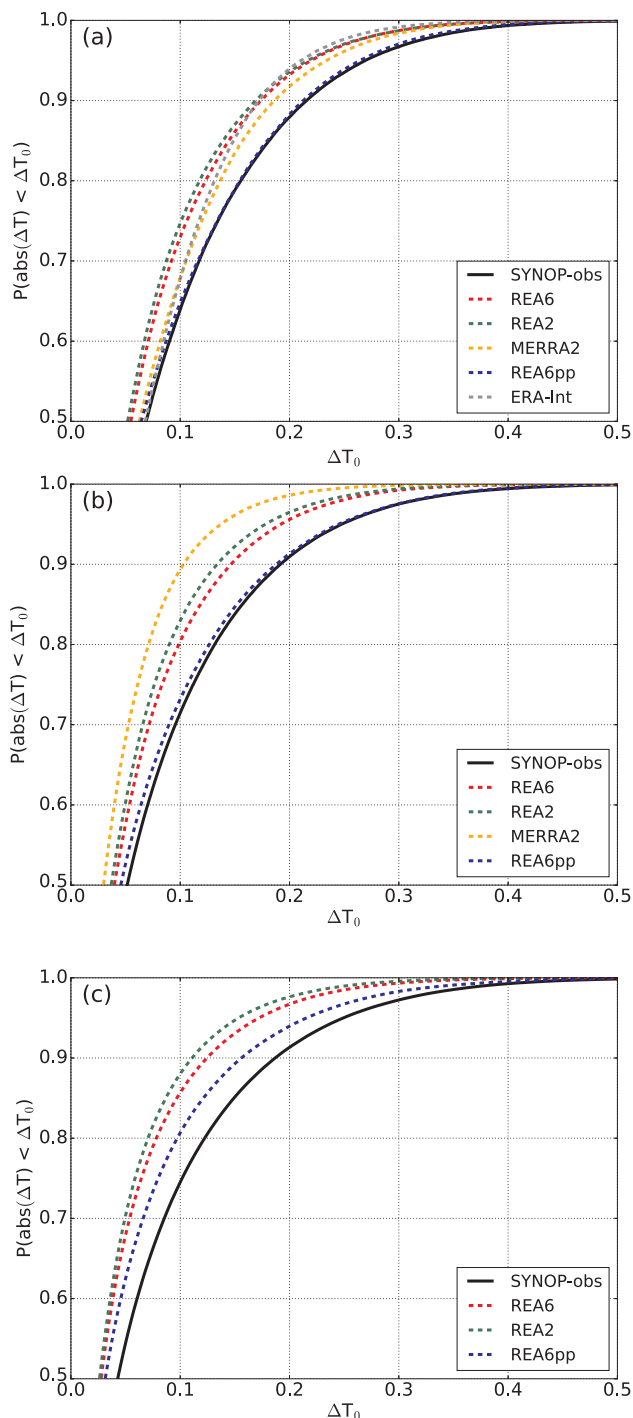


Fig. 12. Cumulative distribution functions of ramp rates in transmissivity. Ramp rates are shown for (a) 3 h averages to compare with ERA-INT, (b) 1 h averages, and (c) 30 min averages.

## 6. Summary

We present a novel post-processed radiation data set based on the high resolution reanalysis COSMO-REA6 that covers Europe over two decades (1995–2014) with 15 min temporal and 6 km horizontal resolution. A first evaluation of the original reanalysis data set using quality-controlled measurements of the Baseline Surface Radiation Network (BSRN) revealed systematic underestimation under clear sky conditions and overestimation during cloudy conditions. The reasons for these discrepancies originate from the aerosol climatology which causes too strong solar extinction and the underestimation of the optical depth of clouds, respectively.

A post-processing scheme was developed to correct for these systematic deficits in COSMO-REA6. In order to separate clear sky and cloudy conditions a transmissivity threshold of 0.5 is used that has been identified with the help of simultaneous GHI and ceilometer observations. As part of the post-processing, scaling factors were estimated by linear orthogonal distance regressions between COSMO-REA6 and BSRN transmissivities. To account for the annual cycle as well as different solar elevation angles, scaling factors were derived for different seasons and solar angles. An optimized weighting function was determined to ensure a smooth transition between clear and cloudy sky conditions.

The post-processing coefficients are based on observations at eight BSRN stations fulfilling the highest quality requirements and covering all major European climate zones. While a further improvement of the developed post-processing approach might be achieved by using a larger number of observation sites, we decided to only use the eight BSRN sites which come with high quality standards as recommended by Gueymard and Myers (2009). The scaling factors are estimated by using a joint data set of all available BSRN sites. Although this procedure reduces the individual site performance in the post-processing, the approach is supposed to minimize local effects and therefore enhances the overall spatial performance of the post-processing. Cross-validation results show the potential of the deduced post-processed data set with a general reduction of systematic biases and a better representation of measured variance for independent locations. This is also valid for independent verification sites exhibiting strongly deviating climate

regimes compared to the measurements in the training data set.

As most other GHI products are available on coarser temporal resolution, the relative performance of COSMO-REA6 is analyzed in terms of daily mean GHI. The novel data set COSMO-REA6pp clearly outperforms the global reanalyses ERA-Interim and MERRA-2 with a lower bias and mean absolute error (MAE), i.e. bias of  $1.8 \text{ W m}^{-2}$  and MAE of  $16.8 \text{ W m}^{-2}$ . When comparing the performance of COSMO-REA6pp for daily mean GHI with those from other studies, i.e. Posselt et al. (2012), Boilley and Wald (2015), the COSMO-REA6pp performance seems to be superior to most satellite and global reanalysis products with the exception of the SARAH satellite data set (Müller et al., 2015). The highest benefit of COSMO-REA6pp compared to global reanalyses is its ability to resolve smaller cloud systems and therefore better represent the spatio-temporal GHI variability. By using measurements from independent German observation sites a higher correlation for spatial GHI difference compared to ERA-Interim was demonstrated.

A ramp rate analysis was done to show the potential of reanalyses to represent small scale variability. The post-processing improves the representation of GHI changes at different time-scales compared to COSMO-REA6 and outperforms ERA-Interim and MERRA-2. The observed ramp rate statistics are well represented by COSMO-REA6pp up to a temporal resolution of 1 h. On smaller time-scales the performance decreases and ramp rates are underestimated by all reanalyses.

In summary, we found a superior performance of COSMO-REA6 in representing observed GHI compared to global reanalyses ERA-Interim and MERRA-2. Further, the post-processed product COSMO-REA6pp was found to represent the observed GHI distribution more realistically. In particular, clear sky radiation amounts are improved.

## 7. Conclusion

The new COSMO-REA6pp GHI is recommended for all applications considering absolute values of GHI. In particular, not only slightly aggregated value investigations (intra-day) will profit from the post-processed GHI, because of the significantly improved clear sky radiation (particularly important for solar energy production studies) and the better representation of GHI ramp rates. However, since many renewable energy studies are using the individual radiation components, direct and diffuse radiation, we will investigate the individual components in one of our next studies.

With respect to renewable energy applications, the regional reanalysis COSMO-REA6 provides not only GHI but also the necessary meteorological parameters, e.g., wind speed at various heights, temperature, precipitation, in a spatio-temporally consistent fashion covering a time period of 20 years. With the new post-processed radiation fields accounting for the shortcomings in the original COSMO-REA6 radiation representation, the overall data set represents a valuable source of information to scientific, governmental as well as commercial users. COSMO-REA6 as well as the post-processed radiation data is available for download via the COSMO Regional Reanalysis website<sup>3</sup>.

## Acknowledgments

This study was performed in the framework of the Hans-Ertel-Centre for Weather Research (Simmer et al., 2016; Weissmann et al., 2014) funded by the German Federal Ministry for Transportation and Digital Infrastructure (Grant No. BMVI/DWD DWD2014P5A). The work is also supported by the Energy Transition and Climate Change Project (ET-CC) at University of Cologne (Grant No. ZUK 81/1). The authors would like to thank Gerd König-Langlo and the Baseline Surface Radiation Network for providing the high quality measurements of radiation, which are crucial for studies like this.

## References

- Bett, P.E., Thornton, H.E., 2016. The climatological relationships between wind and solar energy supply in Britain. *Renew. Energy* 87, 96–110.
- Bett, P.E., Thornton, H.E., Clark, R.T., 2013. European wind variability over 140 yr. *Adv. Sci. Res.* 10 (April), 51–58. URL <<http://www.adv-sci-res.net/10/51/2013/>> .
- Blanc, P., Gschwind, B., Lefèvre, M., Wald, L., 2011. The helioclim project: surface solar irradiance data for climate applications. *Rem. Sens.* 3 (2), 343–361.
- Boilley, A., Wald, L., 2015. Comparison between meteorological re-analyses from ERA-Interim and MERRA and measurements of daily solar irradiation at surface. *Renew. Energy* 75, 135–143. <http://dx.doi.org/10.1016/j.renene.2014.09.042>.
- Bollmeyer, C., Keller, J.D., Ohlwein, C., Wahl, S., Crewell, S., Friederichs, P., Hense, A., Keune, J., Kneifel, S., Pscheidt, I., Redl, S., Steinke, S., 2015. Towards a high-resolution regional reanalysis for the European CORDEX domain. *Quart. J. Roy. Meteorol. Soc.* 141 (686), 1–15. <http://dx.doi.org/10.1002/qj.2486>.
- Borsche, M., Kaiser-Weiss, A.K., Kaspar, F., 2016. Wind speed variability between 10 and 116m height from the regional reanalysis COSMO-REA6 compared to wind mast measurements over Northern Germany and the Netherlands. *Adv. Sci. Res.* 13 (November), 151–161. URL <<http://www.adv-sci-res.net/13/151/2016/>> .
- Cannon, D., Brayshaw, D.J., Methven, J., Coker, P.J., Lenaghan, D., 2014. Using reanalysis data to quantify extreme wind power generation statistics: a 33 year case study in Great Britain. *Renew. Energy* 75, 767–778. <http://dx.doi.org/10.1016/j.renene.2014.10.024>.
- Dee, D., Uppala, S., Simmons, A., Berrisford, P., Poli, P., Kobayashi, S., Andrae, U., Balmaseda, M., Balsamo, G., Bauer, P., et al., 2011. The era-interim reanalysis: configuration and performance of the data assimilation system. *Q. J. Roy. Meteorol. Soc.* 137 (656), 553–597.
- Grams, C.M., Beerli, R., Pfenninger, S., Staffell, I., Wernli, H., 2017. Balancing Europe's wind-power output through spatial deployment informed by weather regimes. *Nature Clim. Change* 7 (8), 557–562.
- Gueymard, C.A., Myers, D.R., 2009. Evaluation of conventional and high-performance routine solar radiation measurements for improved solar resource, climatological trends, and radiative modeling. *Sol. Energy* 83 (2), 171–185. URL <<http://dx.doi.org/10.1016/j.solener.2008.07.015>> .
- Heide, D., von Bremen, L., Greiner, M., Hoffmann, C., Speckmann, M., Bofinger, S., 2010. Seasonal optimal mix of wind and solar power in a future, highly renewable Europe. *Renew. Energy* 35 (11), 2483–2489.
- Heimo, A., Vernez, A., Wasserfallen, P., 1993. Baseline surface radiation network (bsrn). Concept and implementation of a bsrn station.
- Henckes, P., Knaut, A., Obermüller, F., Frank, C., 2018. The benefit of long-term high resolution wind data for electricity system analysis. *Energy* 143, 934–942.
- Jia, B., Xie, Z., Dai, A., Shi, C., Chen, F., 2013. Evaluation of satellite and reanalysis products of downward surface solar radiation over East Asia: spatial and seasonal variations. *J. Geophys. Res. Atmos.* 118 (9), 3431–3446.
- Kaiser-Weiss, A.K., Kaspar, F., Heene, V., Borsche, M., Tan, D.G.H., Poli, P., Obregon, A., Gregow, H., 2015. Comparison of regional and global reanalysis near-surface winds with station observations over Germany. *Adv. Sci. Res.* 12, 187–198. URL <<http://www.adv-sci-res.net/12/187/2015/>> .
- Kleissl, J., 2013. *Solar Energy Forecasting and Resource Assessment*. Academic Press.
- Koepke, P., Hess, M., Schulz, I., Shettle, E.P., 1997. Global Aerosol Dataset. Tech. rep., Max-Planck-Institut für Meteorologie, Hamburg, Germany. URL <[http://www.mpimet.mpg.de/~/MPI-Report\\_243.pdf](http://www.mpimet.mpg.de/~/MPI-Report_243.pdf)> .
- Kohavi, R., 1995. A study of cross-validation and bootstrap for accuracy estimation and model selection. In: *International Joint Conference on Artificial Intelligence*, vol. 14(12), pp. 1137–1143.
- König-Langlo, G., Sieger, R., Schmithüsen, H., Bücker, A., Richter, F., Dutton, E., October 2013. The Baseline Surface Radiation Network and its World Radiation Monitoring Centre at the Alfred Wegener Institute. URL <<http://www.wmo.int/pages/progcos/Publications/gcos-174.pdf>> .
- Kubik, M.L., Brayshaw, D.J., Coker, P.J., Barlow, J.F., 2013. Exploring the role of reanalysis data in simulating regional wind generation variability over Northern Ireland. *Renew. Energy* 57, 558–561. <http://dx.doi.org/10.1016/j.renene.2013.02.012>.
- Linares-Rodríguez, A., Ruiz-arias, J.A., Pozo-vázquez, D., Tovar-pescador, J., 2011. Generation of synthetic daily global solar radiation data based on ERA-Interim reanalysis and artificial neural networks. *Energy* 36 (8), 5356–5365. <http://dx.doi.org/10.1016/j.energy.2011.06.044>.
- Lohmann, S., Schillings, C., Mayer, B., Meyer, R., 2006. Long-term variability of solar direct and global radiation derived from ISCCP data and comparison with reanalysis data. *Solar energy* 80 (11), 1390–1401.
- Long, C.N., Dutton, E.G., 2002. BSRN Global Network recommended QC tests, V2. URL <<http://bsrn.awi.de>> .
- Markovsky, I., Huffel, S.V., 2007. Overview of total least-squares methods. *ScienceDirect* 87, 2283–2302.
- Michaelsen, J., 1987. Cross-Validation in Statistical Climate Forecast Models.
- Molod, A., Takacs, L., Suarez, M., Bacmeister, J., 2015. Development of the GEOS-5 atmospheric general circulation model: evolution from MERRA to MERRA2. *Geosci. Model Dev.* 8 (5), 1339–1356.
- Mulder, F.M., 2014. Implications of diurnal and seasonal variations in renewable energy generation for large scale energy storage. *J. Renew. Sustain. Energy* 033105 (2014), 1–14.
- Müller, R., Pfeifroth, U., Träger-Chatterjee, C., Trentmann, J., Cremer, R., 2015. Digging the METEOSAT treasure3 decades of solar surface radiation. *Rem. Sens.* 7 (6), 8067–8101.
- Ohmura, A., Gilgen, H., Hegner, H., Müller, G., Wild, M., Dutton, E., Forgan, B., Fröhlich,

<sup>3</sup> <http://reanalysis.meteo.uni-bonn.de>

- C., Philipona, R., Heimo, A., König-Langlo, G., McArthur, B., Pinker, R., Whitlock, C., Dehne, K., 1998. Baseline surface radiation network (BSRN/WCRP): new precision radiometry for climate research. *Bull. Am. Meteorol. Soc.* 79, 2115–2136.
- Pfenninger, S., Staffell, I., 2016. Long-term patterns of European PV output using 30 years of validated hourly reanalysis and satellite data. *Energy* 114, 1251–1265.
- Posselt, R., Mueller, R.W., Stöckli, R., Trentmann, J., 2012. Remote sensing of solar surface radiation for climate monitoring - the CM-SAF retrieval in international comparison. *Rem. Sens. Environ.* 118, 186–198. <http://dx.doi.org/10.1016/j.rse.2011.11.016>.
- Rabin, J., Delon, J., Gousseau, Y., 2008. Circular Earth Mover's Distance for the comparison of local features. In: 2008 19th International Conference on Pattern Recognition. pp. 1–4. URL <<http://ieeexplore.ieee.org/document/4761372/>>.
- Randles, C.A., da Silva, A.M., Buchard, V., Darmenov, A., Colarco, P.R., Aquila, V., Bian H., Nowotnick E.P., Pan, X., Smirnov, A., Yu, H., Govindaraju, R., 2016. The MERRA-2 Aerosol Assimilation. Technical Report Series on Global Modeling and Data Assimilation 45 (December 2016). URL <<https://gmao.gsfc.nasa.gov/pubs/docs/Randles887.pdf>>.
- Ranjha, R., Svensson, G., Tjernström, M., Semedo, A., 2013. Global distribution and seasonal variability of coastal low-level jets derived from ERA-Interim reanalysis. *Tellus A: Dynam. Meteorol. Oceanogr.*, 65.
- Richardson, D.B., Andrews, R.W., 2014. Validation of the MERRA dataset for solar PV applications. In: 2014 IEEE 40th Photovoltaic Specialist Conference, PVSC 2014, pp. 809–814.
- Rienecker, M.M., Suarez, M.J., Gelaro, R., Todling, R., Bacmeister, J., Liu, E., Bosilovich, M.G., Schubert, S.D., Takacs, L., Kim, G.K., Bloom, S., Chen, J., Collins, D., Conaty, A., Da Silva, A., Gu, W., Joiner, J., Koster, R.D., Lucchesi, R., Molod, A., Owens, T., Pawson, S., Pegion, P., Redder, C.R., Reichle, R., Robertson, F.R., Ruddick, A.G., Sienkiewicz, M., Woollen, J., 2011. MERRA: NASA's modern-era retrospective analysis for research and applications. *J. Clim.* 24 (14), 3624–3648.
- Ritter, B., Geleyn, J.-F., 1992. A Comprehensive Radiation Scheme for Numerical Weather Prediction Models with Potential Applications in Climate Simulations. URL <<http://journals.ametsoc.org>>.
- Ritter, M., Shen, Z., Cabrera, B.L., Odening, M., Deckert, L., 2015. A new approach to assess wind energy potential. *Energy Proc.* 75, 671–676. <http://dx.doi.org/10.1016/j.egypro.2015.07.485>.
- Rose, S., Apt, J., 2015. What can reanalysis data tell us about wind power? *Renew. Energy* 83, 963–969. <http://dx.doi.org/10.1016/j.renene.2015.05.027>.
- Santos-Alamillos, F.J., Pozo-Vázquez, D., Ruiz-Arias, J.A., Lara-Fanego, V., Tovar-Pescador, J., 2012. Analysis of spatiotemporal balancing between wind and solar energy resources in the southern Iberian Peninsula. *J. Appl. Meteorol. Climatol.* 51 (11), 2005–2024.
- Schättler, U., Doms, G., 2011. A Description of the Nonhydrostatic Regional COSMO-Model Part I: Dynamics and Numerics. Tech. Rep., Deutscher Wetterdienst.
- Simmer, C., Adrian, G., Jones, S., Wirth, V., Gber, M., Hohenegger, C., Janjic, T., Keller, J., Ohlwein, C., Seifert, A., Trömel, S., Ulbrich, T., Wapler, K., Weissmann, M., Keller, J., Masbou, M., Meilinger, S., Ri, N., Schomburg, A., Vormann, A., Weingartner, C., 2016. Herz: The german hans-ertel centre for weather research. *Bull. Am. Meteorol. Soc.* 97 (6), 1057–1068.
- Staffell, I., Pfenninger, S., 2016. Using bias-corrected reanalysis to simulate current and future wind power output. *Energy* 114, 1224–1239. <http://dx.doi.org/10.1016/j.energy.2016.08.068>.
- Stone, M., 1974. Cross-validated choice and assessment of statistical predictions. *J. Roy. Stat. Soc.* 36 (2), 111–147.
- Tanré, D., Geleyn, J.F., Slingo, J., 1984. First results of the introduction of an advanced aerosol-radiation interaction in the ECMWF low resolution global model. In: *Aerosols and Their Climatic Effects*. A. DEEPAC Publishing, pp. 133–177.
- von Storch, H., Zwiers, R.W., 2003. *Statistical Analysis Climate Research*, netlibrary Edition. Cambridge University Press. URL <http://www.cambridge.org>.
- Wahl, S., Bollmeyer, C., Crewell, S., Figura, C., Friederichs, P., Hense, A., Keller, J.D., Ohlwein, C., 2017. A novel convective-scale regional reanalyses COSMO-REA2: improving the representation of precipitation. *Meteorol. Zeitschrift* 26 (4), 345–361. <http://dx.doi.org/10.1127/metz/2017/0824>.
- Weissmann, M., Göber, M., Hohenegger, C., Janjic, T., Keller, J., Ohlwein, C., Seifert, A., Trömel, S., Ulbrich, T., Wapler, K., Bollmeyer, C., Deneke, H., 2014. Initial phase of the Hans-Ertel Centre for Weather Research? A virtual centre at the interface of basic and applied weather and climate research. *Meteorol. Zeitschrift* 23(3), 193–208.
- Zubler, E.M., Lohmann, U., Lüthi, D., Schär, C., 2011. Intercomparison of aerosol climatologies for use in a regional climate model over Europe. *Geophys. Res. Lett.* 38 (15), 1–5.